miR-200 deficiency promotes lung cancer metastasis by activating Notch signaling in cancer-associated fibroblasts

Bin Xue,[1] Chen-Hua Chuang,[2] Haydn M. Prosser,[3,4] Cesar Seigi Fuziwara,[1,5] Claudia Chan,[1] Neil Sahasrabudhe,[1] Maximilian Kühn,[1] Yalei Wu,[6] Jingqi Chen,[1] Anne Biton,[7,8] Caifu Chen,[6] John Erby Wilkinson,[9] Michael T. McManus,[10] Allan Bradley,[3,4] Monte M. Winslow,[2] Bo Su,[11] and Lin He[1]

[1]Division of Cellular and Developmental Biology, Molecular and Cell Biology Department, University of California at Berkeley, Berkeley, California 94705, USA; [2]Department of Genetics, Stanford University School of Medicine, Stanford, California 94305, USA; [3]The Wellcome Trust Sanger Institute, Hinxton, Cambridge CB10 1SA, United Kingdom; [4]Cambridge Institute of Therapeutic Immunology and Infectious Disease, Department of Medicine, University of Cambridge, Cambridge CB2 0AW, United Kingdom; [5]Department of Cell and Developmental Biology, Institute of Biomedical Sciences, University of São Paulo, São Paulo 05508-000, Brazil; [6]Thermo Fisher Scientific, South San Francisco, California 94080, USA; [7]Department of Statistics, University of California at Berkeley, Berkeley, California 94705, USA; [8]Bioinformatics and Biostatistics, Department of Computational Biology, USR 3756, Centre National de la Recherche Scientifique, Institut Pasteur, Paris 01 45 68 80 00, France; [9]Department of Pathology, University of Michigan Medical School, Ann Arbor, Michigan 48109, USA; [10]Department of Microbiology and Immunology, University of California at San Francisco Diabetes Center, W.M. Keck Center for Noncoding RNAs, University of California at San Francisco, San Francisco, California 94143, USA; [11]Central Laboratory, Shanghai Pulmonary Hospital, Tongji University School of Medicine, Shanghai 200433, China

Lung adenocarcinoma, the most prevalent lung cancer subtype, is characterized by its high propensity to metastasize. Despite the importance of metastasis in lung cancer mortality, its underlying cellular and molecular mechanisms remain largely elusive. Here, we identified *miR-200* miRNAs as potent suppressors for lung adenocarcinoma metastasis. *miR-200* expression is specifically repressed in mouse metastatic lung adenocarcinomas, and *miR-200* decrease strongly correlates with poor patient survival. Consistently, deletion of *mir-200c/141* in the *Kras*$^{LSL\text{-}G12D/+}$; *Trp53*$^{flox/flox}$ lung adenocarcinoma mouse model significantly promoted metastasis, generating a desmoplastic tumor stroma highly reminiscent of metastatic human lung cancer. *miR-200* deficiency in lung cancer cells promotes the proliferation and activation of adjacent cancer-associated fibroblasts (CAFs), which in turn elevates the metastatic potential of cancer cells. *miR-200* regulates the functional interaction between cancer cells and CAFs, at least in part, by targeting Notch ligand Jagged1 and Jagged2 in cancer cells and inducing Notch activation in adjacent CAFs. Hence, the interaction between cancer cells and CAFs constitutes an essential mechanism to promote metastatic potential.

[*Keywords*: Jag1; Jag2; cancer-associated fibroblasts; lung cancer; metastasis; miR-200; miR-200c; miR-141; miRNA; microenvironment]

Supplemental material is available for this article.

Received March 9, 2021; revised version accepted June 23, 2021.

Lung adenocarcinoma, the most prevalent lung cancer subtype, is characterized by its high propensity to metastasize. Metastatic lung adenocarcinoma cells escape primary tumors, disseminate via blood and lymphatic circulation, and ultimately colonize distant organs, particularly the liver, bones, and brain (Budczies et al. 2015; Obenauf and Massagué 2015). Metastasis leads to rapid disease progression and organ failure, accounting for the majority of patient mortality (Chaffer and Weinberg 2011). Despite its immense clinical significance, the cellular and molecular basis for lung adenocarcinoma metastasis remains largely unknown.

Both cancer cell intrinsic mechanisms and tumor-stroma interactions regulate metastatic progression (Quail and Joyce 2013). Previous studies have mostly focused on intrinsic metastasis mechanisms that increase

Corresponding authors: lhe@berkeley.edu, su_bo_s@hotmail.com
Article published online ahead of print. Article and publication date are online at http://www.genesdev.org/cgi/doi/10.1101/gad.347344.120.

© 2021 Xue et al. This article is distributed exclusively by Cold Spring Harbor Laboratory Press for the first six months after the full-issue publication date (see http://genesdev.cshlp.org/site/misc/terms.xhtml). After six months, it is available under a Creative Commons License (Attribution-NonCommercial 4.0 International), as described at http://creativecommons.org/licenses/by-nc/4.0/.

chromosome instability and accessibility, promote developmental plasticity, alter the cancer secretome, or enhance epithelial–mesenchymal transition (EMT) (Winslow et al. 2011; Celià-Terrassa and Kang 2016). However, emerging evidence has implicated interactions between cancer cells and the tumor microenvironment, as lung adenocarcinoma metastases are frequently characterized by desmoplasia and substantial remodeling of the tumor microenvironment (Bremnes et al. 2011; Altorki et al. 2019). One major obstacle in studying lung adenocarcinoma metastasis is the limited number of faithful in vivo models that recapitulate the entire metastatic processes. Widely used transplantation models largely depend on cancer cell lines, often bypassing important in vivo processes to achieve metastatic growth (Gómez-Cuadrado et al. 2017); popular genetically engineered mouse models of lung adenocarcinoma often require a long latency to develop metastasis (Jackson et al. 2005; DuPage et al. 2009).

One of the most widely used models for metastatic lung adenocarcinoma is the $Kras^{LSL\text{-}G12D/+}$; $Trp53^{flox/flox}$ (*KP*) model, in which inducible $Kras^{G12D}$ expression and *p53* deletion initiate the growth of lung adenocarcinomas (Jackson et al. 2005). While this model can eventually manifest metastatic tumors that highly resemble human pathology, its usefulness is hampered by long latency and incomplete penetrance (Jackson et al. 2005; DuPage et al. 2009). Here, we identified *miR-200* miRNAs as key suppressors for metastasis in *KP* lung adenocarcinomas. Engineered *miR-200* deficiency promoted rapid metastasis to lymph nodes and distant organs, faithfully recapitulating the desmoplastic tumor microenvironment in metastatic human disease. *miR-200* deficiency in neoplastic cells increases the expression of Notch ligand Jag1 and Jag2. Enhanced Notch signaling in neighboring stromal fibroblasts induced their proliferation and their remodeling into cancer-associated fibroblasts (CAFs), which in turn promoted metastases. Our findings uncover key miRNAs that suppress metastasis by restricting CAF activation, and highlight the role of tumor microenvironment remodeling in lung cancer metastasis.

Results

Down-regulation of miR-200 *miRNAs in a mouse model for metastatic lung cancer*

To compare the miRNA expression profiles between primary and metastatic lung adenocarcinomas, we used the $Kras^{LSL\text{-}G12D/+}$;$Trp53^{flox/flox}$;$R26^{LSL\text{-}tdTomato/+}$ (*KPT*) lung adenocarcinoma mouse model, in which inducible *Kras* activation and *p53* loss in lung epithelial cells yield malignant lung adenocarcinomas with a long latency for metastasis (Jackson et al. 2005; DuPage et al. 2009). Primary tumors and spontaneous metastases from peritoneum, liver, adrenal gland, and soft tissue were collected 5–9 mo after tumor initiation induced by lenti-Cre administration (Winslow et al. 2011). These *KPT* primary tumors may or may not have metastatic potential. *KPT* lung cancer cells were marked with the tdTomato Cre-reporter, which enabled isolation of cancer cells (Fig. 1A). Among 641 miRNAs analyzed, 20 highly expressed miRNAs were differentially expressed between primary tumors and metastases (Fig. 1B; Supplemental Fig. S1A; Supplemental Table S1). Strikingly, nearly all *miR-200* miRNAs were repressed in metastases (Supplemental Fig. S1A). In particular, *miR-141* and *miR-200c* were among the most down-regulated miRNAs in *KPT* metastases (Fig. 1B; Supplemental Fig. S1A).

The *miR-200* family contains five evolutionarily conserved miRNAs in two genomic loci, *mir-200b/200a/429* (chromosome 4) and *mir-200c/141* (chromosome 6). They are classified into two subfamilies that differ by one nucleotide in seed sequences (Fig. 1C). *miR-200* miRNAs were expressed in both early and late stage primary lung adenocarcinomas, exhibiting only a slight down-regulation during tumor progression (Fig. 1D). However, *miR-200*s were strongly repressed in metastatic lung adenocarcinomas in *KPT* mice (Fig. 1D). Consistently, in the 432 human lung adenocarcinomas in TCGA, a collective, low *miR-200* level was correlated with poor patient survival ([***] $P = 0.0018$) (Fig. 1E). Hence, down-regulation of *miR-200* is associated with tumor metastasis in lung adenocarcinomas.

miR-200 *deficiency promotes the development of lung cancer metastases*

We next investigated the role of *miR-200* miRNAs in lung cancer metastasis in the $Kras^{LSL\text{-}G12D/+}$;$Trp53^{flox/flox}$ (*KP*) mouse model. We engineered individual deletion of *mir-200c/141* or *mir-200b/200a/429* in mice (Supplemental Fig. S1B; Prosser et al. 2011). *mir-200c/141*$^{-/-}$ mice were phenotypically normal, deficiency of *mir-200b/200a/429* impaired fertility (Hasuwa et al. 2013), and *mir-200c/141*$^{-/-}$; *mir-200b/200a/429*$^{-/-}$ mice are lethal (data not shown). While further deletion of *mir-200c/141* in *KP* mice (*KP;mir-200c/141*$^{-/-}$, designated as *KP200c*) exhibits only partial *miR-200* deficiency, it nonetheless provides essential insights into the role of *miR-200* in lung cancer metastases.

Upon tumor initiation with Adeno-Cre virus (5×10^6 PFU/mouse), *KP200c* mice quickly developed highly malignant lung adenocarcinomas. Advanced lesions with severe pleomorphic nuclei were present as early as 1 mo after tumor initiation (Supplemental Fig. S1C). At the same time point, *KP* mice only had adenomas with mild nuclei atypia (Supplemental Fig. S1C). At 12 wk, Cre-transduced cells developed into significantly larger and more aggressive lung adenocarcinomas in *KP200c* mice (Supplemental Fig. S1D), with a tumor burden five times as high as that of *KP* mice (Fig. 1G–I). Nearly all *KP200c* tumors were grade 2 or above, with >63% between grades 3 and 5. In comparison, only 27% *KP* tumors were grade 3 or above (Fig. 1I). High-grade *KP200c* tumors were characterized by a large size, a solid histological pattern, large and pleomorphic nuclei, and high degree of desmoplastic stroma (Fig. 1H). Consistently, *KP200c* mice exhibited a significant decrease in overall survival compared with *KP* mice ([***] $P = 0.0004$) (Fig. 1F; Supplemental Table S2).

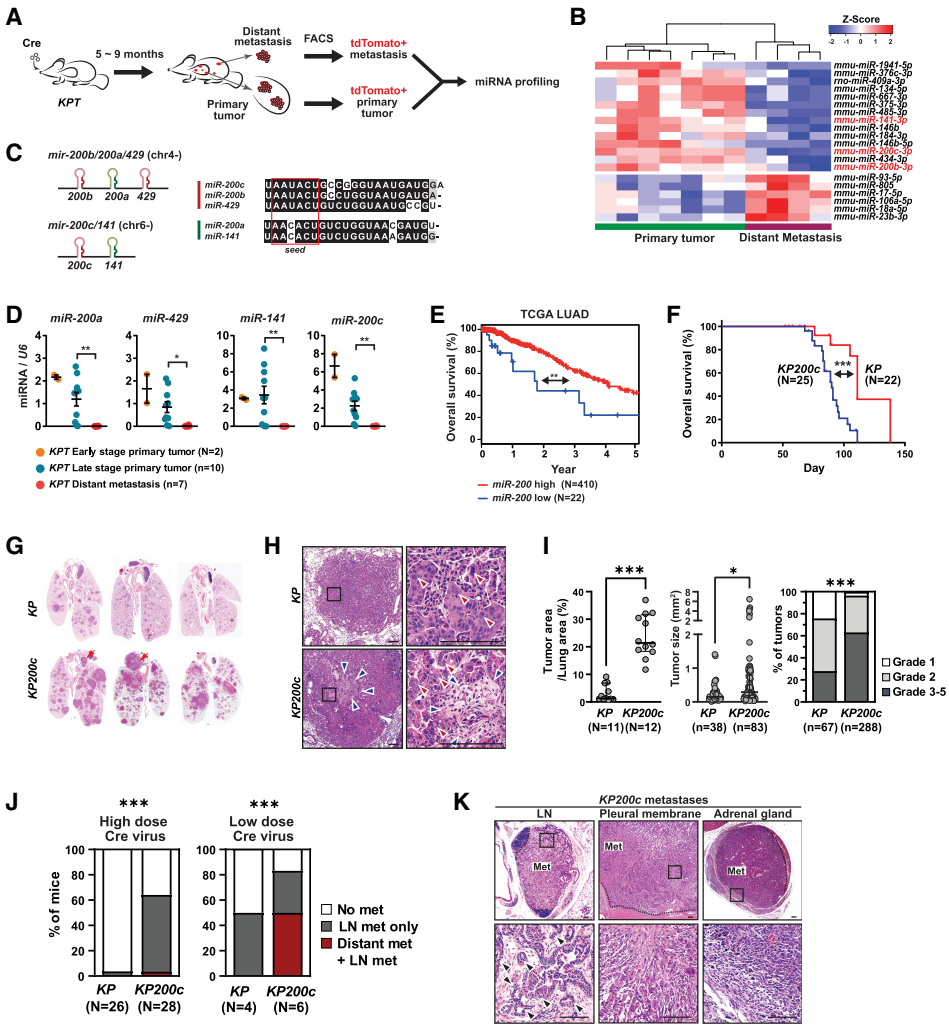

Figure 1. *miR-200* deficiency induces rapid metastasis in *KP* lung cancer model. (*A*) Cartoon illustrating isolation of tdTomato+ cancer cells from primary and metastatic *KPT* lung adenocarcinomas for miRNA profiling. (*B*) *miR-200* miRNAs are strongly down-regulated in distant metastases in the *KPT* mouse lung adenocarcinoma model. A heat map is shown for the most differentially expressed miRNAs between seven *KPT* primary lung tumors and four distant metastases ($P < 0.05$; expression level ≥ -20). (Red text) *miR-200* miRNAs. (*C*) The five *miR-200* miRNAs reside in two genomic loci and segregate into two subfamilies based on seed sequences. Red box, seed sequences. (*D*) *miR-200* miRNAs are strongly down-regulated in metastatic *KPT* tumors. Real-time PCR detected *miR-200* expression in *KP* early stage primary tumors ($N = 2$) and late stage primary tumors ($n = 10$), but not in *KP* metastases ($n = 7$). Error bars indicate SEM. Late stage primary tumors versus metastases. *miR-200a*: (**) $P = 0.0052$, $t = 3.268$, $df = 15$; *miR-429*: (*) $P = 0.0113$, $t = 2.887$, $df = 15$; *miR-141*: (**) $P = 0.01$, $t = 2.047$, $df = 15$; *miR-200c*: (**) $P = 0.0068$, $t = 3.395$, $df = 10$. All statistical analyses were performed using unpaired, two tailed, Student's *t*-test. (*E*) Decreased total *MIR-200* expression human lung adenocarcinomas is associated with poor patient survival in the TCGA data (LUAD). A Kaplan-Meier plot compares patient survival between two cohort of patients, with either high ($N = 410$) or low ($N = 22$) expression of all five *MIR-200* miRNAs. (**) $P = 0.00188$, log rank test. (*F*) *miR-200c/141* deficiency in the *KP200c* model significantly reduces overall survival. A Kaplan-Meier plot compares survival of *KP* and *KP200c* mice after Adeno-Cre administration (5×10^6 Ad-Cre PFU/mouse), demonstrating a significant acceleration of tumor progression in *KP200c* mice. (***) $P = 0.0004$, log rank test. (*G*) *miR-200c/141* deficiency in *KP200c* mice induces a significant increase in tumor progression. Representative H&E staining of lung sections are shown for three pairs of *KP* and *KP200c* mice collected at 90 d after tumor initiation. (Red arrows) Lymph node metastases. (*H*) *KP200c* primary tumors are characterized by desmoplastic stroma (blue arrows) and pleomorphic nuclei in cancer cells (red arrows). Representative images are shown for a pair of late stage *KP* and *KP200c* primary tumors collected at terminal stage. Scale bars, 100 µm. (*I*) *miR-200* deficiency leads to a significant increase in tumor burden, tumor size, and tumor grade in *KP200c* mice. (*Left*) Tumor burden is quantified as the percentage of tumor area versus total lung area. Error bars indicate SEM. (***) $P < 0.001$. (*N*) Animal number, unpaired two-tailed Student's *t*-test, $t = 8.199$, $df = 21$. (*Middle*) Tumor size was measured by tumor area. Error bars indicate SEM. (*) $P = 0.0245$. (*n*) Tumor number, unpaired two-tailed Student's *t*-test, $t = 2.278$, $df = 118$. (*Right*) Tumor grade was determined by histopathological scores. (*n*) Tumor number. (***) $P < 0.001$, $\chi^2 = 70.33$, $df = 2$. All *KP* and *KP200c* tumors were collected at 12 wk after tumor initiation. (*J*) *KP200c* mice exhibit a greater metastasis frequency compared with *KP* mice. Twenty-six *KP* and 28 *KP200c* mice were compared upon tumor initiation with high-dose Cre virus (5×10^6 Ad-Cre PFU/mouse, [***] $P < 0.001$, $\chi^2 = 156.3$, $df = 2$), with *KP200c* mice developing more LN metastases. Four *KP* and six *KP200c* mice were compared upon tumor initiation with low-dose Cre virus (1×10^5 Lenti-Cre PFU/mouse, [***] $P < 0.001$, $\chi^2 = 2428$, $df = 2$), with *KP200c* mice developing more distant metastases. (*K*) *KP200c* mice develop metastases in multiple sites. Representative images of H&E staining of a lymph node metastasis, a pleural metastasis, and a distant metastasis in adrenal gland from *KP200c* mice are shown. Dotted line shows the boundary of metastasis and normal tissue. Scale bar, 100 µm.

miR-200c/141 deficiency not only accelerated tumor growth and progression, but also increased the metastasis frequency. More than 60% of *KP200c* mice ($n = 28$) developed lymph node (LN) metastases within 120 d, mostly affecting mediastinal and thoracic lymph nodes (Fig. 1G,J; Supplemental Table S2). Within 120 d, only 4% *KP* mice (n = 26) developed LN metastasis (Fig 1J). When a lower dose of Adeno-Cre virus initiates tumors in *KP200c* and *KP* mice (1×10^5 Lenti-Cre PFU/mouse), 50% of *KP200c* mice developed full-blown distant metastases to liver, pleura, pericardium, and adrenal gland by 150 d (Fig. 1J, K; Supplemental Fig. S1F; Supplemental Table S2), and *KP* mice exhibited much lower primary tumor burden with no distant metastasis (Fig. 1J; Supplemental Table S2). Interestingly, all *KP200c* metastases exhibited a complete silencing of *mir-200b/200a/429* (Supplemental Fig. S1E), indicating a strong selective pressure for a complete *miR-200* loss. Hence, *KP200c* mice provide a powerful experimental system to probe the underlying mechanisms of adenocarcinoma metastasis.

miR-200 *deficiency induces the expansion of CAFs in metastatic* KP200c *tumors*

Metastases in *KP200c* mice were accompanied by an increase in MAPK signaling and a loss of cell differentiation (Fig. 2A). Compared with *KP* primary tumors, phosphorylated Erk1/2 level was significantly increased in *KP200c* primary tumors ([*] $P = 0.0263$), and further elevated in *KP200c* LN and distant metastases ([***] $P < 0.0001$) (Fig. 2A). In addition, 64% of *KP200c* lymph node and distant metastases were negative for surfactant protein C (SPC), a marker for type 2 alveolar epithelial cells (AT2), and club cell antigen 10 (CC10), a marker for bronchiolar club cells (Fig. 2B). *KP200c* primary tumors, in comparison, were more heterogeneous in SPC and CC10 expression, with only 28% of tumors being $SPC^{low}CC10^{low}$ (Fig. 2B; Supplemental Fig. S2A). Nearly all *KP200c* metastases lost expression of Nkx2.1 (Fig. 2C), a lung lineage transcription factor that controls cellular differentiation and limits metastatic potential (Winslow et al. 2011). *KP200c* primary tumors, however, mostly expressed Nkx2.1, with a down-regulated expression in high-grade tumors (Fig. 2C). Hence, *KP200c* metastases could be derived from poorly differentiated cancer cells with highly elevated MAPK signaling.

A prominent cellular hallmark of metastatic *KP200c* tumors was the abundance of collagen-rich, stromal desmoplasia within the metastatic tumor microenvironment. In comparison, *KP* tumors only exhibited widespread desmoplasia in rare lymph node and liver metastases, but not in the primary tumors (Supplemental Fig. S2B–S2D). The desmoplastic tumors are enriched in CAFs, a heterogeneous population of fibroblasts that can promote cancer growth, survival, and invasiveness by secreting cytokines and growth factors (interleukins, HGF, CXCLs, TGF-β, etc.) (Bhowmick et al. 2004; Orimo et al. 2005; Kalluri and Zeisberg 2006; Frantz et al. 2010; Pietras and Östman 2010; Gascard and Tlsty 2016; Ahirwar et al. 2018), as well as collagen to increase tissue stiffness (Pankova et al. 2016). In *KP200c* late stage primary tumors, lymph node metastases, and distant metastases, we observed a marked increase of α-smooth muscle actin-expressing CAFs (α-SMA+ CAFs) (Fig. 2D), which grew into multiple layers with stress-fiber-like feature intertwined with clusters of *KP200c* cancer cells (Fig. 2D). This α -SMA+ stromal structure was largely absent in *KP* primary tumors, including high-grade tumors where α-SMA+ cells are thin single layer (Fig. 2D). Unlike α-SMA+ CAFs, FSP-1-expressing CAFs did not show a significant increase in *KP200c* tumors (Supplemental Fig. S2E). Importantly, the percentage of α-SMA+ CAFs in lymph node metastasis was proportional to the tumor size in *KP200c* metastases, but not in *KP* metastases (Fig. 2E), with 70% of *KP200c* lymph node metastases containing at least 20% of α-SMA+ CAFs (Fig. 2E). α-SMA staining was absent from the epithelial compartment in both *KP* and *KP200c* normal lung and early lesions (Fig. 2F). Moreover, the CAFs in the advanced *KP200c* tumors were derived from untransduced cells shown by the absence of tdTomato expression (Supplemental Fig. S1D). Our findings suggest that *miR-200* deficiency in lung adenocarcinomas lead to the recruitment and expansion of α-SMA+ CAFs in tumor microenvironment, which could be a critical step for developing metastatic lung adenocarcinomas.

In *KP200c* mice, both neoplastic cells and stromal cells were deficient for *mir-200c/141*. Hence, it is unclear whether *mir-200c*/141 deficiency in cancer cells and/or stromal cells drove tumor growth and metastasis. To address the role of mir-200c/141 specifically in neoplastic cells, we generated *KP* mice with a *mir-200c/141* conditional allele ($Kras^{G12D/+}$; $p53^{flox/flox}$; $mir\text{-}200c/141^{flox/-}$, designated as *KP200cCKO* mice) (Park et al. 2012). This model generates *mir-200c/141*-deficient *KP* cancer cells in an otherwise *mir-200c/141*-wild type tumor microenvironment (Supplemental Fig. S2F). Similar to *KP200c* mice, *KP200cCKO* mice exhibited an increase in metastasis frequency, with 80% of *KP200cCKO* mice developing lymph node or distant metastases by 120 d (Fig. 2G; Supplemental Table S2; Supplemental Fig. S2G). Metastases in *KP200cCKO* mice were also characterized by strong desmoplasia with extensive infiltration of α-SMA+ CAFs (Fig. 2G). Hence, *miR-200* deficiency in lung cancer cells promotes local and distant metastases, while inducing the expansion of α-SMA+ CAFs in the tumor microenvironment.

Enrichment of SMA+ CAFs occurs in human metastatic lung adenocarcinomas

Consistent with α-SMA+ CAF enrichment in metastatic *KP200c* mouse lung tumors, α-SMA+ CAFs are also enriched in metastatic human lung adenocarcinomas (Fig. 3A). We compared α-SMA staining in paired primary lung adenocarcinomas and lymph node metastases ($n = 8$) and observed a significant increase of α-SMA+ CAFs in lymph node metastases (Fig. 3A). Two patients exhibited a similar enrichment of α-SMA+ CAFs in liver metastases relative to their paired primary tumors (Fig. 3B).

Interestingly, we captured a continuum of CAF activation patterns in a stage IA human lung adenocarcinoma

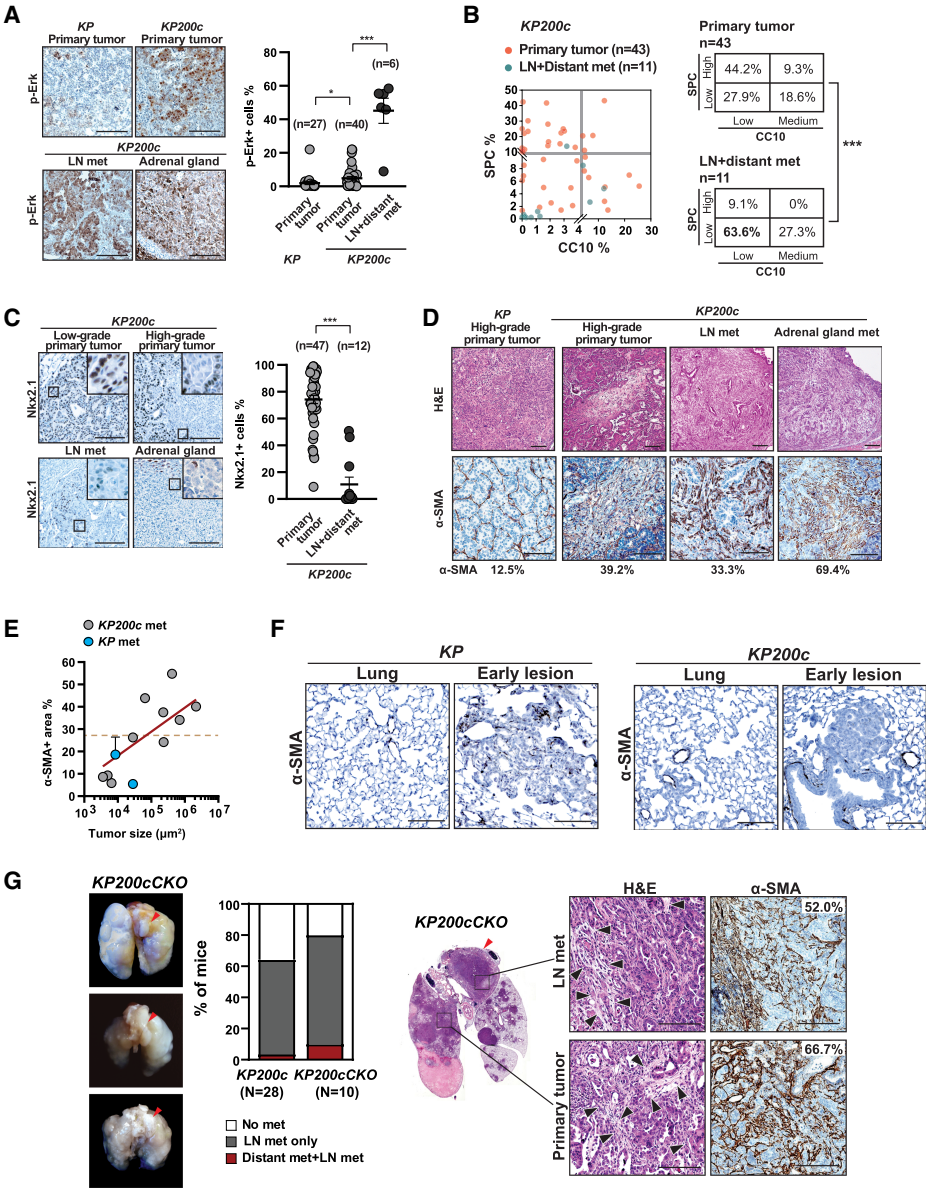

Figure 2. CAFs are enriched in metastatic *KP200c* lung adenocarcinomas. (*A*) Primary and metastatic *KP200c* tumors exhibit a strong increase in MAPK signaling. Immunohistochemistry staining of phosphorylated Erk1/2 (p-Erk) (*left*) and quantitation of p-Erk-positive cells (*right*) indicate a strong elevation of MAPK signaling in *KP200c* tumors, particularly the metastatic *KP200c* tumors. Twenty-seven *KP* primary tumors, 40 *KP200c* primary tumors and 6 *KP200c* metastases were analyzed. Scale bar, 100 μm. Error bar indicates SEM. *KP* versus. *KP200c* primary tumor. (*) $P = 0.0263$, unpaired two-tailed Student's *t*-test, $t = 2.273$, $df = 65$; *KP200c* primary versus *KP200c* lymph node metastases, (***) $P < 0.0001$, unpaired two-tailed Student's *t*-test, $t = 11.06$, $df = 44$. (*B*) Metastatic *KP200c* tumors are characterized by a loss of cell lineage markers. (*Left*) Quantitation is shown for immunohistochemistry staining of CC10 (a marker for Club cells) and SPC (a marker for alveolar type 2 cells) in *KP200c* primary and metastatic tumors. Tumor stratification shows a preferential loss of CC10 and SPC expression in *KP200c* metastases compared with *KP200c* primary tumors. *KP200c* primary tumors versus metastases. (***) $P < 0.0001$, $\chi^2 = 61.67$, $df = 3$. (*C*) Metastatic *KP200c* tumors exhibit a down-regulation of Nkx2.1. Representative images (*left*) and quantitation (*right*) of Nkx2.1 immunohistochemistry staining are shown for *KP200c* primary tumors, lymph node, and distant metastases. Scale bar, 100 μm. Error bar indicates SEM. (***) $P < 0.0001$, unpaired two-tailed Student's *t*-test, $t = 9.474$, $df = 57$. Forty-seven *KP200c* primary tumors and 12 *KP200c* metastases (both lymph node and distant metastases) were analyzed. (*D*,*E*) α-SMA-expressing CAFs are enriched in *KP200c* primary tumors and metastases. (*D*) Representative images of H&E and α-SMA staining are shown for high-grade regions of *KP* and *KP200c* primary tumors, as well as *KP200c* metastases. Scale bars, 100 μm. (*E*) Abundance of α-SMA+ CAFs is correlated with the size of *KP200c* metastases. The percentage of α-SMA staining in total tumor area is plotted against the size of metastatic tumors for 10 *KP200c* lymph node metastases and two *KP* lymph node metastases, A simple linear regression line against *KP200* metastases is superimposed. $R^2 = 0.3599$. (*F*) α-SMA positive fibroblasts are absent from *KP* and *KP200c* normal lung and early primary tumors. Representative images of α-SMA staining are shown for *KP* and *KP200c* normal lung and early primary tumors. Scale bars, 100 μm. (*G*) Deficiency of *miR-200c/141* specifically in cancer cells promotes metastasis progression and desmoplastic stroma. (*Left*) *KP200cCKO* lungs collected 90 d after tumor initiation (5×10^6 Adeno-Cre PFU/mouse) exhibit evident lymph node metastases, with metastasis frequency comparable with that of *KP200c* mice. (*Right*) H&E and α-SMA staining of high-grade regions of *KP200cCKO* primary tumors and lymph node metastases indicate strong CAF enrichment in the tumor microenvironment. Scale bars, 100 μm.

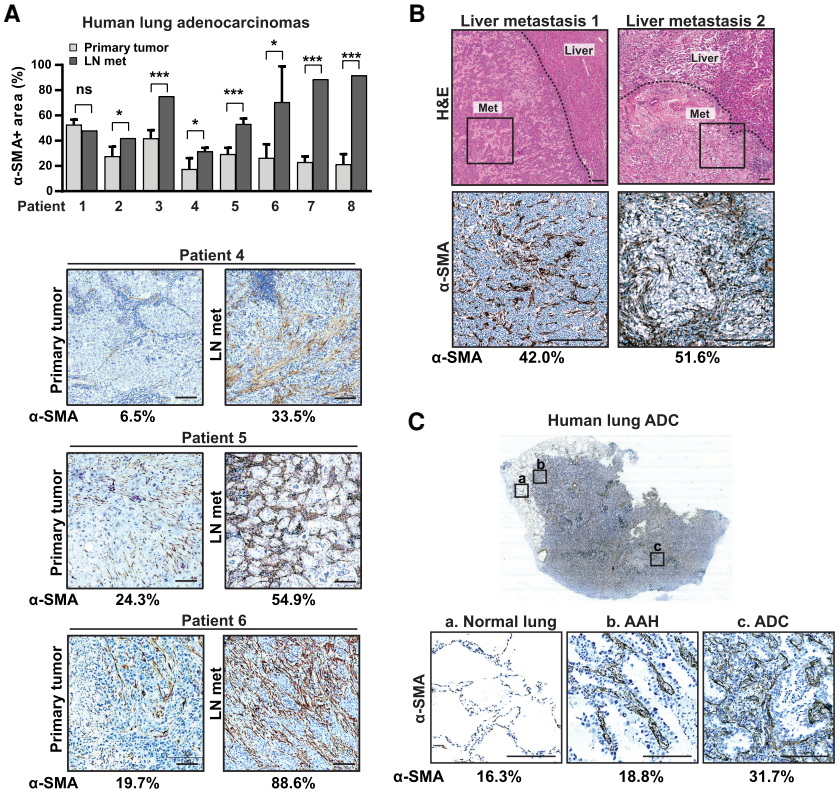

Figure 3. Enrichment of SMA+ CAFs occurs in human metastatic lung adenocarcinomas. (*A*,*B*) Human metastatic lung adenocarcinomas exhibit an increase of α-SMA+ CAFs compared with paired primary tumors. (*A*) Quantitation of α-SMA+ area is shown for eight pairs of human primary and metastatic lung adenocarcinomas; representative immunohistochemistry staining images are shown for three pairs. Scale bars, 100 µm. Pair 1: (ns) $P = 0.0661$, $t = 2.509$, $df = 4.000$; pair 2: (*) $P = 0.0148$, $t = 4.101$, $df = 4.000$; pair 3: (***) $P = 0.0004$, $t = 11.22$, $df = 4.000$; pair 4: (*) $P = 0.0467$, $t = 2.883$, $df = 3.869$; pair 5: (***) $P = 0.0010$, $t = 6.955$, $df = 4.951$; pair 6: (*) $P = 0.0250$, $t = 3.530$, $df = 3.920$; pair 7: (***) $P = 0.0001$, $t = 27.80$, $df = 3.000$; pair 8: (***) $P < 0.0001$, $t = 19.42$, $df = 4.000$. All statistical analyses were performed using unpaired two-tailed Student's *t*-test with Welch's correction. (*B*) α-SMA+ CAFs are enriched in liver metastases from relapsed human lung adenocarcinoma patients. H&E staining are shown for two independent liver metastases samples and α-SMA staining are shown for the boxed metastasis region. Dotted line indicates the tumor/liver boundary. Scale bars, 100 µm. (*C*) Increased cancer-CAF interaction is associated with tumor progression in human lung adenocarcinomas. A stage IA lung adenocarcinoma was stained for α-SMA, and regions representing a progressive histopathological pattern including normal lung, atypical adenomatous hyperplasia (AAH), and adenocarcinoma (ADC) are marked and shown magnified. Quantitation of α-SMA+ area was shown. Scale bar, 100 µm.

(Fig. 3C). In normal lung, the thin alveoli septa consist of a monolayer of α-SMA+ pericytes embedded in the basement membrane of type 1 alveolar cells (AT1) (Fig. 3C, panel a). When the lesion progressed to atypical adenomatous hyperplasia (AAH), the transformed epithelial cells grew into the alveolar space with the α-SMA+ CAFs starting to expand within the alveolar septa (Fig. 3C, panel b). In high-grade adenocarcinomas where the alveolar lumen is filled with cancer cells (Fig. 3C, panel c), the α-SMA+ CAFs formed multilayered structures intermingled with cancer cells. Hence, the expansion of the α-SMA+ CAFs in the tumor microenvironment, as well as the extent of tumor-CAF interaction, both correlate with histological progression in human adenocarcinomas.

Fibroblast coculture promotes the metastatic features in KP200c *tumor organoids*

We next established a 3D tumor organoid system by culturing one *KP* and three *KP200c* lung cancer cell lines (Supplemental Fig. S3A) on top of a matrix containing 50% Matrigel + 0.5 mg/mL Collagen I to mimic a collagen-rich lung tumor microenvironment (Fig. 4A). When cultured alone, *KP* and *KP200c* cancer cells both formed well-polarized spherical tumor organoids with hollow lumina (Fig. 4B), with *KP200c* organoids slightly larger in size (Fig. 4B), but with neither exhibiting invasive features (Fig. 4B).

Interestingly, when cocultured with primary lung fibroblasts, the miR-200 deficient *KP200c* organoids, but not the *miR-200*-expressing *KP* organoids, clustered to form large multi-acinar structures with cellular protrusions, indicative of invasive behavior (Fig. 4C,D). This clustering behavior substantially increased the size of *KP200c* tumor organoids (Fig. 4B; Supplemental Fig. S3B). The extent of organoid clustering, along with the degree of cell proliferation and invasiveness in *KP200c* organoids, were proportional to the ratio of fibroblasts to cancer cells (Supplemental Fig. S3C). Consistently, re-expression of *mir-200c/141* in *KP200c* cancer cells reverted this invasive phenotype when cocultured with lung fibroblasts, restoring a spherical organoid morphology (Supplemental Fig. S3D,F). Hence, *miR-200* miRNAs act in lung cancer cells to restrict the metastatic phenotype, at least in part, by regulating the functional interaction between cancer cells and fibroblasts.

miR-200 *deficiency in tumors promotes the proliferation and activation of CAFs*

The interaction between *KP200c* cancer cells and stromal fibroblasts induced invasive features in neoplastic cells, while promoting their proliferation in 3D organoid culture (Fig. 4E), but not in 2D culture (Supplemental Fig. S3E). Increased fibroblast proliferation was only observed in the vicinity of *KP200c* tumor organoids (Fig. 4B), as

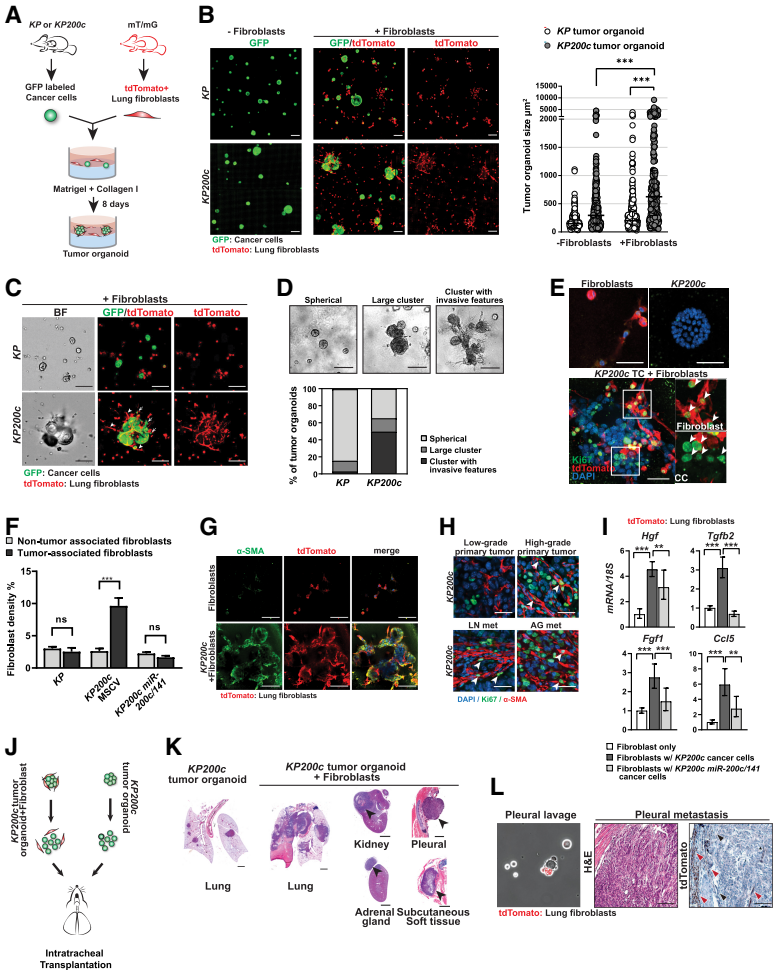

Figure 4. *miR-200* deficiency in cancer cells promotes CAF activation to drive tumor metastasis. (*A*) A diagram illustrating the tumor-fibroblast organoid coculture model. GFP-labeled *KP* or *KP200c* lung cancer cells are cocultured with tdTomato labeled normal lung fibroblasts to form tumor organoids. (*B–D*) *miR-200* deficiency in *KP* cancer cells induces metastatic features upon coculture with lung fibroblasts. (*B*) Fluorescence images (*left*) and quantitation (*right*) of tumor-fibroblast organoids indicate that *miR-200* deficiency in *KP* cancer cells, combined with fibroblast coculture, induced tumor clustering and promoted metastatic cellular features. Scale bar, 100 µm. *KP200c* alone versus *KP200c* + fibroblasts, (***) $P < 0.0001$, $t = 7.404$, $df = 568$; *KP200c* + fibroblasts versus *KP* + fibroblasts, (***) $P < 0.0001$, $t = 7.894$, $df = 488$; unpaired two-tailed Student's *t*-test. (*C*,*D*) Representative images and quantification are shown for clustering and invasiveness in *KP* and *KP200c* tumor organoids with fibroblast coculture. Scale bars, 100 µm. (*C*) *KP200c* organoids exhibit invasive features in cancer cells (arrows) and elongated morphology in cocultured fibroblasts (arrowheads). (*D*) Analysis of 87 *KP* and 112 *KP200c* tumor organoids indicate a strong increase in invasive features in *KP200c* tumor organoids. (*E*) Ki67 immunostaining in *KP200c* organoid with fibroblast coculture indicates strong cell proliferation in both cancer cells and fibroblasts (tdTomato+). Scale bar, 100 µm. (White arrowheads) Ki67+ cells. (*F*) *miR-200* re-expression in *KP200c* cancer cells decreases cell proliferation of tumor-associated lung fibroblasts in organoid coculture, but fails to affect non-tumor-associated fibroblasts. The tdTomato signal coverage was measured. Error bar indicates SD. Non-tumor-associated fibroblasts versus tumor-associated fibroblasts: *KP*: (ns) $P = 0.3823$, $t = 1.021$, $df = 3$; *KP200c*-MSCV: (***) $P = 0.0006$, $t = 6.484$, $df = 6$; *KP200c*-MSCV-*miR-200c/141*: (ns) $P = 0.2456$, $t = 1.440$, $df = 3$, unpaired two-tailed Student's *t*-test. (*G*) Coculture of *KP200c* cancer cells and lung fibroblasts in organoids promotes α-SMA induction in fibroblasts. Scale bars, 100 µm. (*H*) Increased α-SMA+ CAF proliferation is observed in *KP200c* high-grade primary tumors and metastatic tumors, but not in *KP200c* MSCV low-grade primary tumors. Low-grade primary tumors, high-grade primary tumors, lymph node metastases, and adrenal gland metastases from *KP200c* mice were immunostained for Ki67 and α-SMA. White arrowheads, proliferating CAFs (Ki-67+, α-SMA+). Scale bars, 20 µm. (*I*) *miR-200* expression in *KP200c* cancer cells regulates the induction of specific cytokine and growth factors by CAFs. Control *KP200c* cancer cells enhanced fibroblast production of prometastatic cytokines and growth factors including *Hgf*, *Tgfb2*, *Fgf1* and *Ccl5*, while *miR-200* re-expression in *KP200c* cancer cells reversed this phenotype. Error bar indicates SD. All statistical analyses are performed using unpaired, two-tailed Student's *t*-test. (*J*,*K*) *KP200c* cancer cells primed with lung fibroblasts yield highly metastatic lung tumors in an orthotropic allograft tumor model 4 wk after tumor transplantation. (*J*) A cartoon illustrating the orthotropic allograft model to study lung cancer metastasis using cocultured *KP200c* cancer cells and lung fibroblasts. (*K*) H&E staining reveals a highly metastatic tumor phenotype in primary tumors, lymph node metastases, and distant metastases generated from *KP200c* cancer cells primed by lung fibroblast coculture. Scale bar, 500 µm, black arrowheads, metastases. (*L*) Transplanted exogenous fibroblasts and endogenous fibroblasts from recipient mice both contribute to CAFs in metastatic tumor microenvironment. Disseminating tumor clusters from pleural cavity and pleural metastasis both contain transplanted tdTomato+ CAFs and endogenous tdTomato– CAFs. Scale bar, 100 µm. (Red arrowheads) tdTomato+ CAFs, (black arrowheads) tdTomato- CAFs.

tumor-associated fibroblasts exhibited a 3.8-fold increase in cell density compared with non-tumor-associated fibroblasts (Fig. 4F). No proliferation difference was observed between *KP* tumor-associated and non-tumor-associated fibroblasts (Fig. 4F). *KP200c* tumor-associated fibroblasts exhibited elongated morphology, induction of α-SMA, and infiltration into tumor organoids to form direct cell-cell contact with cancer cells (Fig. 4G). Consistently, highly proliferative α-SMA+ CAFs with an elongated morphology were prevalent in *KP200c* high-grade primary tumors, lymph nodes, and distant metastases, but not in low-grade primary tumors (Fig. 4H; Supplemental Fig. S3G).

miR-200 deficiency in lung cancer cells not only promotes the proliferation of surrounding lung fibroblasts, but also regulates their activity. A major function of CAFs is to secrete cytokines, chemokines, and growth factors to promote tumor growth, survival, and invasion (Gascard and Tlsty 2016). We isolated tdTomato+ lung fibroblasts that were cultured alone or cocultured with *KP200c* tumor organoids, and compared their expression

of CAF-derived secreted factors. Fibroblasts cocultured with *KP200c* tumor organoids exhibited a strong induction of hepatocyte growth factor (HGF), TGF-β, fibroblast growth factor-1 (Fgf1) and Ccl5 (Fig. 4I), all of which have been reported to contribute to metastatic potential in different cancer models including lung adenocarcinoma (Ao et al. 2007; Karnoub et al. 2007; Borczuk et al. 2008; Kojima et al. 2010; Straussman et al. 2012; Yu et al. 2015; Sun et al. 2017). Interestingly, *mir-200c/141* re-expression in *KP200c* tumor organoids reduced the induction of these growth factors and cytokines in cocultured fibroblasts (Fig. 4I), suggesting that *miR-200* miRNAs in cancer cells regulate CAF gene expression via a cell-nonautonomous mechanism. Moreover, treating *KP200c* cancer cells with HGF, TGF-β, or a combination of both is sufficient to induce the invasive behavior, resulting in enlarged invasive tumor organoid clusters (Supplemental Fig. S3H).

Interplay between KP200c *cancer cells and fibroblasts promotes metastatic potential in vivo*

Our findings implicate a complex interplay between cancer cells and CAFs regulated by *miR-200* miRNAs. To investigate the importance of cancer–fibroblast interactions in promoting metastases, we established an orthotropic allograft lung tumor model in which we intratracheally transplanted lung cancer cells with or without primary lung fibroblasts into immune deficient recipient mice (Fig. 4J). Among two *KP* and three *KP200c* lung cancer lines tested, *KP* lines rarely grafted to form tumors, yet all *KP200c* lines successfully developed allograft lung tumors by 7 wk (Supplemental Fig. S3I). When *KP200c* cancer cells were injected with cocultured, tdTomato-labeled, primary lung fibroblasts, tumor growth was significantly accelerated with an increased tumor burden (Fig. 4K; Supplemental Fig. S3J). More importantly, within a short latency of 40 d, all mice exhibited early onset distant metastases affecting the pleural membrane in rib cage, pericardium, adrenal gland, kidney, and subcutaneous soft tissue (Fig. 4K; Supplemental Fig. S3K). In comparison, mice injected with *KP200c* cancer cells alone, while developing lung tumors, rarely developed metastases at this time point (Fig. 4K; Supplemental Fig. S3K). These allograft *KP200c* tumors likely gain metastatic potential eventually, as they promoted the proliferation and activation of endogenous stromal fibroblasts in recipient mice. Altogether, our data demonstrate that boosting cancer-fibroblast interactions in *KP200c* cancer cells significantly accelerated tumor outgrowth and metastases in vivo.

Surprisingly, when *KP200c* cancer cells were cotransplanted with primary lung fibroblasts into recipient mice, tdTomato+ fibroblasts could be detected within the disseminating cancer cell clusters in the pleural cavity and in distant metastases (Fig. 4L). Similarly, in *KP200c* mice, we observed cancer cell clusters that contained α-SMA+ CAFs inside blood/lymphatic vessels in the lung (Supplemental Fig. S3L). Consistently, in a human patient with minimally invasive lung adenocarcinomas and lymph node micrometastases, we detected clusters of cells containing α-SMA+ CAFs adjacent to CK19+ cancer cells in blood (Supplemental Fig. S3M), and observed lymph node micrometastases encased by a single layer of α-SMA+ CAFs in the vicinity of lymphatic vessels (Supplemental Fig. S3N). These findings suggest that α-SMA+ CAFs can adhere to metastatic cancer cells during dissemination and extravasation, and prolonged tumor-CAF interaction could play a role throughout different stages of tumor metastasis.

miR-200 *miRNAs repress* Jag1/Jag2 *and inhibit Notch signaling in CAFs to repress metastasis*

Cancer cells can convert lung fibroblasts into tumor-promoting CAFs via paracrine signaling or direct cell-cell interactions. Interestingly, *KP200c* cancer cells induced lung fibroblast proliferation and activation in a tumor organoid coculture system that permitted cell-cell contact, but not in *trans*-well assays that separated cancer cells and fibroblasts in different compartments to prohibit cell-cell contacts (Fig. 5A). Hence, *miR-200* miRNAs likely regulate pathways for direct cell-cell interactions between cancer cells and CAFs.

Many studies suggest that a key function of *miR-200* miRNAs is to suppress EMT by targeting *Zeb1* and *Zeb2* (Korpal et al. 2008; Park et al. 2008; Gibbons et al. 2009; Gregory et al. 2011). However, primary and metastatic *KP200c* tumors remained largely intact in epithelial morphology (Supplemental Fig. S4A), and failed to exhibit *miR-200*-dependent regulation of Zeb1, Zeb2, vimentin, and E-cadherin (Supplemental Fig. S4B,C). Furthermore, *Zeb1* and *Zeb2* knockdown in *KP200c* lung cancer cells did not alter the invasive morphology of *KP200c* tumor organoids (Supplemental Fig. S4D,E). We cannot exclude the possibility that transient EMT still occurs during lung cancer metastasis *in vivo*, since *miR-200*-deficient lung cancer cells are more susceptible to TGF-β-induced EMT (Gibbons et al. 2009). However, our data strongly suggest that the *miR-200*-EMT pathway is not required for cancer-CAF interactions that play an essential role in promoting metastasis.

Gene ontology analysis on predicted *miR-200* targets revealed multiple candidates involved in cell-cell communication, including *Jagged1* (*Jag1*), *Jagged2* (*Jag2*), *Postn*, *Gjc1,* and *Pcdh9,* as predicted by RNA22 and TargetScan algorithms (Miranda et al. 2006; Agarwal et al. 2015). Notch ligands *Jag1 and Jag2* emerged as strong candidate *miR-200* targets, each containing a predicted *miR-141* or *miR-200c* binding site, respectively (Fig. 5B). Furthermore, *Jag1 and Jag2* mRNA expression was elevated in *miR-200*-deficient metastatic cancer cells (Fig. 5C; Supplemental Fig. S1D), but reduced upon *miR-200* re-expression (Fig. 5D). Hence, the di-cistronic miRNA cluster *mir-200c/141* acts coordinately to down-regulate both *Jag1* and *Jag2* expression in cancer cells.

Notch signaling operates in diverse developmental and pathological processes. Notch ligands, including Jag1, Jag2, Dll1, and Dll4, bind to membrane-bound Notch

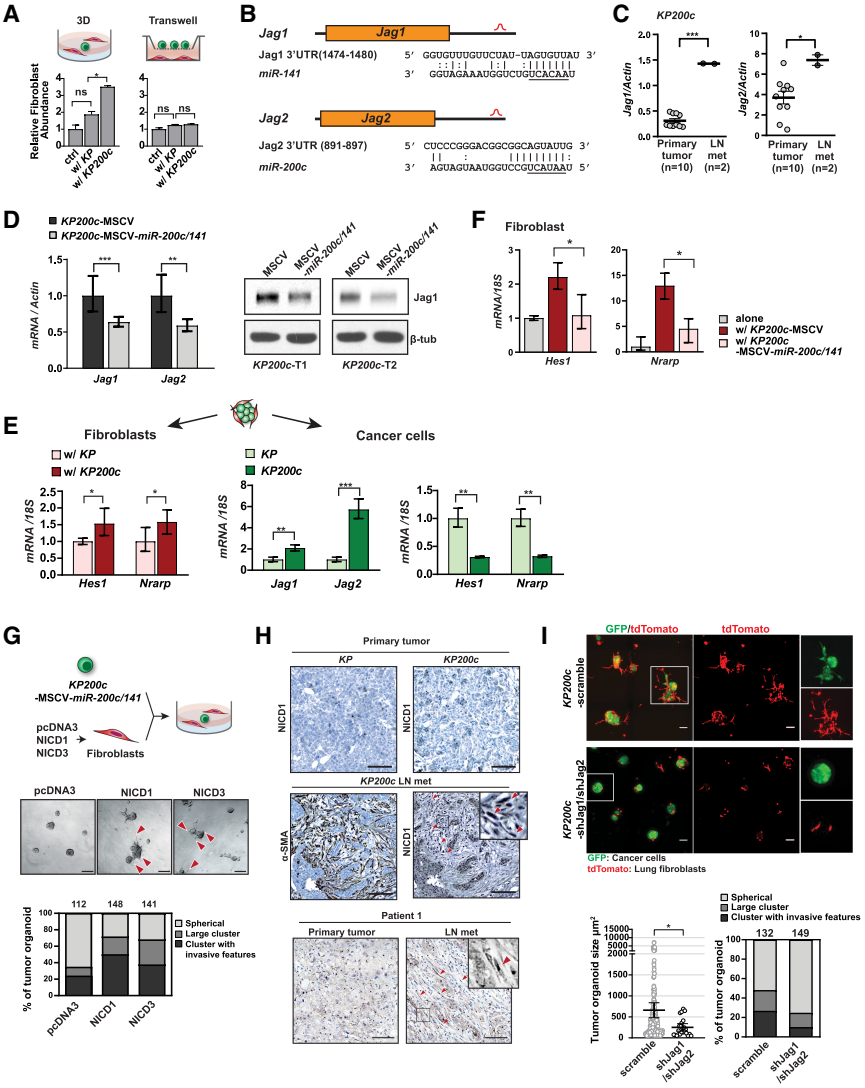

Figure 5. *miR-200* represses *Jag1*/*Jag2* in cancer cells and inhibits Notch signaling in CAFs. (*A*) Direct cell–cell contact mediates the activation of cocultured fibroblasts by *KP200c* cancer cells. *KP200c* cancer cells promote proliferation of fibroblasts only in tumor organoid culture, where direct cell-cell contact was permitted, but not in transwell assays. Error bars indicate SD. Fibroblasts + *KP* tumor organoids versus fibroblasts + *KP200c* tumor organoids, (*) $P = 0.0104$, $t = 3.185$, $df = 2$, unpaired two-tailed Student's *t*-test. (*B*) Candidate *miR-141* and *miR-200c* binding sites in the 3′ UTR of *Jag1* and *Jag2*, respectively, as predicted by TargetScan. (*C*) Metastatic *KP200c* tumors exhibit an induction of *Jag1* and *Jag2* compared with *KP200c* primary tumors. Ten *KP200c* primary tumors and 2 lymph node metastases were subjected to real-time PCR for *Jag1* and *Jag2*. Error bars indicate standard error. *Jag1 KP200c* primary tumor versus LN met: (***) $P < 0.0001$, $t = 12.03$, $df = 10$; *Jag2 KP200c* primary tumor versus LN met: (*) $P = 0.0290$, $t = 2.548$, $df = 10$, unpaired Student's *t*-test. (*D*) Overexpression of *mir-200c/141* in *KP200c* cancer cells suppresses the mRNA (*left*) and protein (*right*) expression of both *Jag1* and *Jag2*. Error bars indicate SD. (*E*) Coculture of lung fibroblasts and *KP200c* cancer cells induces Notch signaling in fibroblasts, but represses Notch signaling in cancer cells. tdTomato+ fibroblasts cocultured with *KP200c* cancer cells in tumor organoid assay exhibit an increase in Notch target genes (*Hes1* and *Nrarp*) compared with those cocultured with *KP* cancer cells. When cocultured with fibroblasts, *KP200c* cancer cells exhibit an increase in *Jag1* and *Jag2* expression, but decrease in Notch target genes compared with *KP* cancer cells. Error bar indicates SD. (*F*) *miR-200* re-expression in *KP200c* cancer cells represses Notch targets *Hes1* and *Nrarp* in cocultured fibroblasts. Error bars indicate SD. All statistical analyses were performed using unpaired, two-tailed Student's *t*-test. (*G*) Activated Notch signaling in fibroblasts promotes metastatic behavior of cocultured, *miR-200* expressing cancer cells. Lung fibroblasts expressing mouse NICD1, NICD3, or control pcDNA3 vector were cocultured with *mir-200c/141* expressing *KP200c* cancer cells, and invasive features of cancer cells were examined by light microscopy. Fibroblasts with activated Notch signaling, but not control fibroblasts, conferred a metastatic phenotype in *miR-200* expressing *KP200c* cancer cells in organoid culture. Scale bars, 100 μm. (Red arrows) Invasive cellular structures in cancer cells cocultured with fibroblasts with activated Notch signaling. Morphology of tumor organoids was quantified as described in Figure 3D. (*H*) Metastatic *KP200c* mouse tumors and metastatic human lung adenocarcinomas both contain CAFs with strong expression of nuclear Notch1, compared with paired primary tumors. Scale bars, 100 μm. Red arrows point to the CAF stained positive for activated Notch1. (*I*) Knockdown of both *Jag1* and *Jag2* in *KP200c* cancer cells inhibits invasiveness in cancer cells and proliferation in fibroblasts when cultured as tumor organoids with lung fibroblasts. *Jag1* and *Jag2* double knockdown in *KP200c* cancer cells, when cocultured with lung fibroblasts, restores a spherical morphology of tumor organoids (*left*), reduces the size of tumor organoids (*middle*), and decreases the invasive features of tumor organoids (*right*). Scale bar, 100 μm.

receptors in neighboring cells, inducing a cascade of proteolytic events that ultimately release the Notch intracellular domain (NICD), which translocates into the nucleus (Artavanis-Tsakonas 1999; Kopan and Ilagan 2009; Bray 2016). In the nucleus, NICD interacts with DNA binding protein RBPJ and coactivator MAML to stimulate the transcription of Notch target genes, such as Hes, Hey, and Nrarp (Lamar et al. 2001; Iso et al. 2003). Notch expressing cells are often activated by cell surface ligands in adjacent cells, and Notch ligand producing cells are known to dampen their own Notch activity through *cis*-inhibition (del Álamo et al. 2011). Consistently, *miR-200* deficiency resulted in elevated expression of Notch ligand *Jag1* and *Jag2* in cancer cells and elevated expression of Notch target genes *Hes1* and *Nrarp* in cocultured fibroblasts, but a decrease in Notch

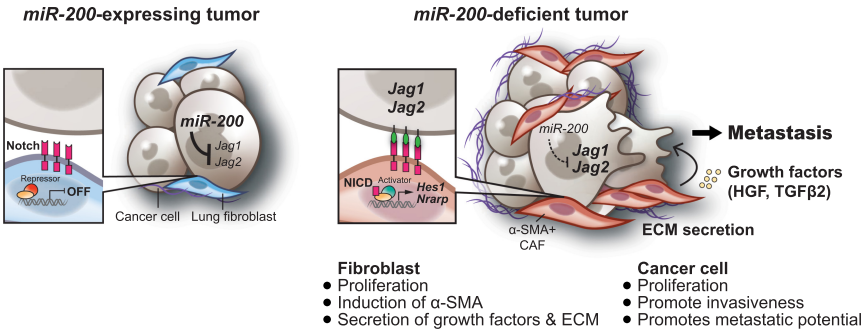

Figure 6. A model illustrating the role of *miR-200* miRNAs in lung cancer metastasis by regulating the interaction between cancer cells and fibroblasts. In *miR-200*-expressing cancer cells, *miR-200* targets *Jag1* and *Jag2*; hence, the cancer cells fail to activate Notch signaling in adjacent fibroblasts and lack metastatic potential. *miR-200* deficiency in cancer cells de-represses *Jag1* and *Jag2*, triggering Notch activation in neighboring CAFs, which promotes fibroblast proliferation and activation, ultimately enhancing the metastatic potential of the cancer cells.

target gene expression in *KP200c* cancer cells (Fig. 5E). This induction of Notch activity in cocultured fibroblasts was reversed by re-expressing *miR-200c/141* in *KP200c* cancer cells (Fig. 5F).

To investigate the sufficiency of elevated fibroblast Notch signaling to promote the metastatic potential of cancer cells, we manipulated Notch signaling in lung fibroblasts and examined their effects on cocultured tumor organoids. Since Notch1 and Notch3 are the main Notch receptors expressed in lung fibroblasts (data not shown), we activated Notch signaling in lung fibroblasts by overexpressing Notch1 NICD (NICD1) or Notch3 NICD (NICD3), and cocultured them with *miR-200c/141-re*-expressing *KP200c* tumor organoids. *miR-200* expression abolished metastatic features of *KP200c* tumor organoids cocultured with normal lung fibroblasts (Supplemental Fig. S3F), yet coculture with NICD1- and NICD3-expressing fibroblasts reversed this *miR-200* effect, promoting cancer cell clustering and invasive cellular features (Fig. 5G). This is likely due to the activation of Notch directly inducing the expression of CAF-related cytokines including *Ccl2, Ccl5, Hgf* and *Tgfb2* (Supplemental Fig. S4H). Consistently, α-SMA+ CAFs in *KP200c* metastases exhibited specific activated Notch1 nuclear staining (Fig. 5H, top), indicative of a strong Notch activation in these cells. Similar observations were made in two human lung adenocarcinoma samples, where activated Notch1 nuclear staining was evident in CAFs associated with metastases (Fig.5H; Supplemental Fig. S4G).

Consistent with *Jag1* and *Jag2* being the key *miR-200* targets that mediate tumor-CAF interactions, knocking down *Jag1* and *Jag2* in *KP200c* cancer cells restored a spherical morphology in tumor organoids, abolished tumor clustering and invasive features, and reduced fibroblasts elongation and expansion (Fig. 5I). Hence, *Jag1* and *Jag2* derepression caused by *miR-200* loss in cancer cells triggered Notch activation in adjacent CAFs, which promoted fibroblast proliferation and activation, ultimately enhancing the metastatic potential of cancer cells (Fig. 6).

Discussion

miR-200 miRNAs act as potent suppressors of lung cancer metastasis, and complete *miR-200* inactivation was observed in metastatic lung adenocarcinomas in both *KP* and *KP200c* models. The *KP200c* model is among the best for studying lung adenocarcinoma metastasis, owing to its short latency and faithful recapitulation of patient pathology. Metastatic *KP200c* lung adenocarcinomas faithfully recapitulate the desmoplastic stroma found in human metastatic tumors (Bremnes et al. 2011), characterized by a prometastatic niche filled with SMA+ CAFs. These SMA+ CAFs, derived from normal lung fibroblasts, strongly foster the metastatic potential of cancer cells, at least in part, by secreting cytokines and growth factors (Fig. 3G,I). A recent study showed that human metastatic lung adenocarcinomas possess transcriptomes encompassing a developmental continuum ranging from stem cell-like cells to regenerative progenitors in lung epithelia (Laughney et al. 2020). It is likely that CAFs in the desmoplastic microenvironment not only promote tumor cell proliferation, but also create a prometastatic niche to induce developmental plasticity in cancer cells. This is consistent with the reports that Wnt-expressing fibroblasts establish a stem cell niche for AT2 cells in normal development and for cancer stem cells in lung adenocarcinoma (Tammela et al. 2017; Nabhan et al. 2018). Given the heterogeneity of the tumor microenvironment, CAF-dependent prometastatic niches are likely to require interactions between CAFs and other stromal cell types in lung adenocarcinomas.

In many miR-200 studies, *miR-200* miRNAs are characterized as key inhibitors of EMT by repressing *Zeb1* and *Zeb2* (Korpal et al. 2008; Park et al. 2008; Gibbons et al. 2009; Gregory et al. 2011), acting through a cell intrinsic mechanism to enhance metastasis. However, EMT may not be essential for metastasis in *KP200c* lung adenocarcinomas, as overt EMT was not observed in metastatic *KP200c* tumors, and *Zeb1* and *Zeb2* knockdown failed to reverse invasiveness in tumor organoids (Supplemental Fig. S4A,D,E). Rather, miR-*200* deficiency in *KP200c* cancer cells mediates a cell extrinsic mechanism to alter the interaction between cancer cells and CAFs. *miR-200* deficiency in cancer cells increases Jag1 and Jag2, elevating Notch signaling in neighboring fibroblasts to promote their conversion into highly proliferative, α-SMA+ CAFs, thereby establishing a prometastatic niche. This Notch activation in CAFs is strongly associated with metastatic lung adenocarcinomas in both mouse models and human patients (Fig. 4H), contributing to a prometastatic

microenvironment. Notch signaling regulates fibroblast dependent, cell-cell interactions in multiple lung pathological processes, at least in part, by promoting the secretory factors to remodel microenvironment (Liu et al. 2009). Hence, the *miR-200*/Jag/Notch axis that orchestrates cancer–CAF interactions are likely to constitutes an important regulation to suppress metastasis, additional in vivo studies are needed to verify the Jag/Notch interaction in driving CAF recruitment and cancer metastases.

The effects of Notch signaling are context-dependent in various tumor types. Activation of Notch3 has been shown to mark cancer stem cells and drive self-renewal in *KP* lung cancer mouse model (Zheng et al. 2013). Notch activation in fibroblasts promotes CAF activation and tumor progression in lung, breast, and prostate cancer (Su et al. 2017; Strell et al. 2019), yet the loss of CAF Notch signaling promotes an oncogenic tumor microenvironment in squamous cell carcinomas (Hu et al. 2012; Procopio et al. 2015). It is important to recognize that the unique cellular heterogeneity found within each tumor microenvironment could foster a complex crosstalk between cancer cells and stromal cells, and among different stromal cell types. In both mouse and human metastatic lung adenocarcinomas, *miR-200* deficient lung cancer cells could also induce Notch signaling in other stromal cell types to promote metastasis.

It has been long recognized that highly metastatic lung adenocarcinomas are frequently associated with a prometastatic and desmoplastic tumor microenvironment, characterized by the expansion of cancer associated fibroblasts (CAFs). Here, we demonstrated that *miR-200* is a potent suppressor of tumor metastasis in lung cancer, whose deficiency activates Notch signaling in the tumor microenvironment, particularly CAFs, to remodel tumor microenvironment to favor metastasis.

Materials and methods

Animals

Mice of $Kras^{LSL\text{-}G12D/+}$;$Trp53^{flox/flox}$ genotype were crossed with *mir-200c/141*$^{-/-}$ mice to generate $Kras^{LSL\text{-}G12D/+}$;$Trp53^{flox/flox}$; *mir-200c/141*$^{-/-}$ (*KP200c*) mice (Jackson et al. 2005; Prosser et al. 2011). *KP200c* mice were crossed with *mir-200c/141*$^{flox/flox}$ mice (Park et al. 2012) to generate $Kras^{LSL\text{-}G12D/+}$;$Trp53^{flox/flox}$; *mir-200c/141*$^{flox/-}$ (*KP200cCKO*) mice. Lung tumorigenesis was induced by intranasal instillation of 5×10^6 PFU of recombinant Ad-Cre virus (Gene Transfer Vector Core, University of Iowa) or by intratracheal intubation of 1×10^5 PFU Lenti-Cre virus (DuPage et al. 2009).

Human primary and metastatic tumor samples of lung adenocarcinoma

Matched primary and metastatic tumor samples, blood samples liver metastases and early stage lung tumors were collected from patients, approved by the Institutional Review Board of Shanghai Pulmonary Hospital, School of Medicine, Tongji University. These patients were diagnosed with clinical stage Ia/IIa/IIb/IIIa/IV, pathologically confirmed lung adenocarcinoma.

microRNA analysis

For TaqMan microRNA assay, cDNA was synthesized with preamplification from total RNA using Megaplex RT primers, Megaplex PreAmp primers, TaqMan MicroRNA reverse transcription kit and TaqMan PreAmp master mix kit. Subsequently, quantitative-PCR was carried out using TaqMan array rodent microRNA A + B card set v3.0 (Applied Biosystems 4444909). LUAD data were downloaded from TCGA and normalized using upper quantile. Patients were classified into two groups - "lower" and "higher," according to the expression of the mir-200 family. Survival analysis was performed to compare the two groups, using the package "survival" in R (https://cran.r-project.org/web/packages/survival/index.html). *P*-value was determined by Log rank test, to quantify the significance of the differences in survival time between the two patient groups. Individual microRNA and mRNA were analyzed by real-time PCR using the primers shown in Supplemental Table S3.

Three-dimensional tumor organoid culture for tumor–stromal interaction

The tumor organoid culture was performed using protocol described previously (Debnath et al. 2003) with modifications. Eight-well chamber slides were coated with 100 µL of Matrigel (Corning 354234)/0.5mg/mL Collagen I (Corning 354236) mixture. Tumor cells and fibroblast cells were trypsinized and resuspended in growth media with supplement at twice the desired density and mix with equal volume of 10% Matrigel/Collagen I mixture. The cell/gel mixture were immediately plated on top of the matrix coating and cultured for up to 8 d at 37°C with 5% CO_2.

Orthotopic transplantation experiment

Tumor cells and fibroblast were cocultured as organoids in suspension for 5 d prior to transplantation. On the day of orthotopic transplantation, tumor organoids were dissociated into single cells using trypsin/EDTA, and the percentages of tumor cells and tdTomato+ fibroblasts were determined by FACS. Single-cell suspension containing 1×10^5 tumor cells were resuspended in 50 µL of RPMI1640 with 10 mM EDTA and injected into the lung of *nu/nu* mice (Taconic) by intratracheal intubation. The tumors were collected either at 40 d after the tumor injection or at their terminal stage.

Histopathology and immunohistochemistry

For tumor histology, whole lungs were fixed, dehydrated and embedded in paraffin wax (ACROS Organics). The lung blocks were sectioned at 5-µm thicknesses and stained with hematoxylin and eosin (H&E). Each tumor was given a score of grades 1–5. For IHC, paraffin sections were deparaffinized, dehydrated, and subjected to heat-induced antigen retrieval using Trilogy (Cell Marque 920P). Slides were incubated for 10 min with 3% H_2O_2, blocked with 10% goat serum in PBS + 0.05% Triton X-100, incubated with primary antibody and then horseradish peroxidase (HRP)-conjugated secondary antibodies.

Jag1/Jag2 knockdown

The Jag1 knockdown lentiviral expression vector were constructed into pRRL-SFFV-GFP-miR-E-Puro (SGEP) vector and the Jag2 knockdown lentiviral expression vector were constructed into pRRL-SFFV-GFP-miR-E-Neo (SGEN) vector (Fellmann et al. 2013). The oligo sequences encoding Jag1 and Jag2 shRNA were designed using splashRNA algorithm (Supplemental Table S4;

Pelossof et al. 2017), and cloned into XhoI/EcoRI sites. The shRNA lentiviral vectors were package in HEK293 cells together with pVSV-G and pMD-2 as previously described. Five shRNAs were tested for each gene, and the ones with best knockdown effect were used to generated double knockdown cell line. Cells transduced with both shJag1 and shJag2 were selected 48 h after infection using 2 μg/mL puromycin (Gibco by Thermo Fisher) and 500 μg/mL geneticin (Gibco by Thermo Fisher).

Competing interest statement

The authors declare no competing interests.

Acknowledgments

We thank H. Nolla, H. Kartoosh, and A. Valeros for FACS support; A.M. Li for establishing a collaboration with A. Bradley's laboratory; A. Holly, J.Y. Lee, and F. Ives from Molecular Imaging Center at University of California at Berkeley, and M. West and P. He from High-Throughput Sequencing Facility at University of California at Berkeley for imaging assistance; the Functional Genomics Laboratory at University of California at Berkeley for genomics services; C. Hung for experimental help and proofreading the manuscript; S. Chen for revision advice; G. Lee, A. Nazarenko, T. Colston, and S. Yue for experimental help and mouse colony management; C. Fellmann for providing SGEP and SGEN vectors; M. Junttila, R. Molina, and J. Long from Genentech for intranasal injection protocol; H. Ji and F. Li for *Kras*$^{G12D/+;}$*Lkb1*$^{flox/flox}$ tumor samples; and N. Arpaia, K.A. Kaiser, and all L.H. laboratory members, in particular N. Okada, M. Bennett, E. Ho, and J. Schwedler, for suggestions and discussions. L.H. is a Thomas and Stacey Siebel Distinguished Chair Professor, and is supported by a Howard Hughes Medical Institute (HHMI) Faculty Scholar award, a Bakar Fellow award at University of California at Berkeley, and several grants from the National Institutes of Health (NIH; R01CA139067 and 1R21OD027053). M.M.W. was supported by NIH R01-CA175336 and R01-CA204620. C.-H.C was funded by an American Lung Association Fellowship. C.S.F was funded by Fundacao de Amparo a Pesquisa do Estado de Sao Paulo (FAPESP:2017:01829-0 and 2019/17282-5). M.T.M was supported by 5U01CA217882 and the W.M. Keck Foundation. B.S. was supported by grant number 81572269 from the National Natural Science Foundation of China.

Author contribution: B.X., B.S., M.M.W., and L.H. conceived, designed, and directed the study. B.X. performed most mouse experiments and generated the majority of the mouse data for this study. B.S. performed most experiments involving human samples, and has contributed his clinical expertise to this study. C.-H.C and M.M.W. generated and isolated *KP* tumors and metastases for miRNA analysis. J.C. and A. Biton performed survival analysis of human data from TCGA. J.E.W. performed pathology analysis on all the mouse tumors. C. Chan, N.S., C.S.F., and M.K. performed mouse tumor histology, IHC staining, and molecular cloning experiments. Y.W. and C. Chen designed and provided miRNA TaqMan analysis. H.M.P and A. Bradley generated *miR-200c/141*-null mice. M.T.M. generated *mir-200c/141*^{lacZ} mice. B.X. and L.H. wrote the manuscript with input from all authors.

References

Agarwal V, Bell GW, Nam J-W, Bartel DP. 2015. Predicting effective microRNA target sites in mammalian mRNAs. *Elife* **4:** e05005. doi:10.7554/eLife.05005

Ahirwar DK, Nasser MW, Ouseph MM, Elbaz M, Cuitiño MC, Kladney RD, Varikuti S, Kaul K, Satoskar AR, Ramaswamy B, et al. 2018. Fibroblast-derived CXCL12 promotes breast cancer metastasis by facilitating tumor cell intravasation. *Oncogene* **37:** 4428–4442. doi:10.1038/s41388-018-0263-7

Altorki NK, Markowitz GJ, Gao D, Port JL, Saxena A, Stiles B, McGraw T, Mittal V. 2019. The lung microenvironment: an important regulator of tumour growth and metastasis. *Nat Rev Cancer* **19:** 9–31. doi:10.1038/s41568-018-0081-9

Ao M, Franco OE, Park D, Raman D, Williams K, Hayward SW. 2007. Cross-talk between paracrine-acting cytokine and chemokine pathways promotes malignancy in benign human prostatic epithelium. *Cancer Res* **67:** 4244–4253. doi:10.1158/0008-5472.CAN-06-3946

Artavanis-Tsakonas S. 1999. Notch signaling: cell fate control and signal integration in development. *Science* **284:** 770–776. doi:10.1126/science.284.5415.770

Bhowmick NA, Neilson EG, Moses HL. 2004. Stromal fibroblasts in cancer initiation and progression. *Nature* **432:** 332–337. doi:10.1038/nature03096

Borczuk AC, Papanikolaou N, Toonkel RL, Sole M, Gorenstein LA, Ginsburg ME, Sonett JR, Friedman RA, Powell CA. 2008. Lung adenocarcinoma invasion in TGFβRII-deficient cells is mediated by CCL5/RANTES. *Oncogene* **27:** 557–564. doi:10.1038/sj.onc.1210662

Bray SJ. 2016. Notch signalling in context. *Nat Rev Mol Cell Biol* **17:** 722–735. doi:10.1038/nrm.2016.94

Bremnes RM, Dønnem T, Al-Saad S, Al-Shibli K, Andersen S, Sirera R, Camps C, Marinez I, Busund L-T. 2011. The role of tumor stroma in cancer progression and prognosis: emphasis on carcinoma-associated fibroblasts and non-small cell lung cancer. *J Thorac Oncol* **6:** 209–217. doi:10.1097/JTO.0b013e3181f8a1bd

Budczies J, von Winterfeld M, Klauschen F, Bockmayr M, Lennerz JK, Denkert C, Wolf T, Warth A, Dietel M, Anagnostopoulos I, et al. 2015. The landscape of metastatic progression patterns across major human cancers. *Oncotarget* **6:** 570–583. doi:10.18632/oncotarget.2677

Celià-Terrassa T, Kang Y. 2016. Distinctive properties of metastasis-initiating cells. *Genes Dev* **30:** 892–908. doi:10.1101/gad.277681.116

Chaffer CL, Weinberg RA. 2011. A perspective on cancer cell metastasis. *Science* **331:** 1559–1564. doi:10.1126/science.1203543

Debnath J, Muthuswamy SK, Brugge JS. 2003. Morphogenesis and oncogenesis of MCF-10A mammary epithelial acini grown in three-dimensional basement membrane cultures. *Methods* **30:** 256–268. doi:10.1016/S1046-2023(03)00032-X

del Álamo D, Rouault H, Schweisguth F. 2011. Mechanism and significance of *cis*-inhibition in Notch signalling. *Curr Biol* **21:** R40–R47. doi:10.1016/j.cub.2010.10.034

DuPage M, Dooley AL, Jacks T. 2009. Conditional mouse lung cancer models using adenoviral or lentiviral delivery of Cre recombinase. *Nat Protoc* **4:** 1064–1072. doi:10.1038/nprot.2009.95

Fellmann C, Hoffmann T, Sridhar V, Hopfgartner B, Muhar M, Roth M, Lai DY, Barbosa IAM, Kwon JS, Guan Y, et al. 2013. An optimized microRNA backbone for effective single-copy RNAi. *Cell Rep* **5:** 1704–1713. doi:10.1016/j.celrep.2013.11.020

Frantz C, Stewart KM, Weaver VM. 2010. The extracellular matrix at a glance. *J Cell Sci* **123:** 4195–4200. doi:10.1242/jcs.023820

Gascard P, Tlsty TD. 2016. Carcinoma-associated fibroblasts: orchestrating the composition of malignancy. *Genes Dev* **30:** 1002–1019. doi:10.1101/gad.279737.116

Gibbons DL, Lin W, Creighton CJ, Rizvi ZH, Gregory PA, Goodall GJ, Thilaganathan N, Du L, Zhang Y, Pertsemlidis A, et al. 2009. Contextual extracellular cues promote tumor cell EMT and metastasis by regulating miR-200 family expression. *Genes Dev* **23:** 2140–2151. doi:10.1101/gad.1820209

Gómez-Cuadrado L, Tracey N, Ma R, Qian B, Brunton VG. 2017. Mouse models of metastasis: progress and prospects. *Dis Model Mech* **10:** 1061–1074. doi:10.1242/dmm.030403

Gregory PA, Bracken CP, Smith E, Bert AG, Wright JA, Roslan S, Morris M, Wyatt L, Farshid G, Lim Y-Y, et al. 2011. An autocrine TGF-β/ZEB/miR-200 signaling network regulates establishment and maintenance of epithelial–mesenchymal transition. *Mol Biol Cell* **22:** 1686–1698. doi:10.1091/mbc.e11-02-0103

Hasuwa H, Ueda J, Ikawa M, Okabe M. 2013. MiR-200b and miR-429 function in mouse ovulation and Are essential for female fertility. *Science* **341:** 71–73. doi:10.1126/science.1237999

Hu B, Castillo E, Harewood L, Ostano P, Reymond A, Dummer R, Raffoul W, Hoetzenecker W, Hofbauer GFL, Dotto GP. 2012. Multifocal epithelial tumors and field cancerization from loss of mesenchymal CSL signaling. *Cell* **149:** 1207–1220. doi:10.1016/j.cell.2012.03.048

Iso T, Kedes L, Hamamori Y. 2003. HES and HERP families: multiple effectors of the Notch signaling pathway. *J Cell Physiol* **194:** 237–255. doi:10.1002/jcp.10208

Jackson EL, Olive KP, Tuveson DA, Bronson R, Crowley D, Brown M, Jacks T. 2005. The differential effects of mutant p53 alleles on advanced murine lung cancer. *Cancer Res* **65:** 10280–10288. doi:10.1158/0008-5472.CAN-05-2193

Kalluri R, Zeisberg M. 2006. Fibroblasts in cancer. *Nat Rev Cancer* **6:** 392–401. doi:10.1038/nrc1877

Karnoub AE, Dash AB, Vo AP, Sullivan A, Brooks MW, Bell GW, Richardson AL, Polyak K, Tubo R, Weinberg RA. 2007. Mesenchymal stem cells within tumour stroma promote breast cancer metastasis. *Nature* **449:** 557–563. doi:10.1038/nature06188

Kojima Y, Acar A, Eaton EN, Mellody KT, Scheel C, Ben-Porath I, Onder TT, Wang ZC, Richardson AL, Weinberg RA, et al. 2010. Autocrine TGF-β and stromal cell-derived factor-1 (SDF-1) signaling drives the evolution of tumor-promoting mammary stromal myofibroblasts. *Proc Natl Acad Sci* **107:** 20009–20014. doi:10.1073/pnas.1013805107

Kopan R, Ilagan MXG. 2009. The canonical Notch signaling pathway: unfolding the activation mechanism. *Cell* **137:** 216–233. doi:10.1016/j.cell.2009.03.045

Korpal M, Lee ES, Hu G, Kang Y. 2008. The miR-200 family inhibits epithelial–mesenchymal transition and cancer cell migration by direct targeting of E-cadherin transcriptional repressors ZEB1 and ZEB2. *J Biol Chem* **283:** 14910–14914. doi:10.1074/jbc.C800074200

Lamar E, Deblandre G, Wettstein D, Gawantka V, Pollet N, Niehrs C, Kintner C. 2001. Nrarp is a novel intracellular component of the Notch signaling pathway. *Genes Dev* **15:** 1885–1899. doi:10.1101/gad.908101

Laughney AM, Hu J, Campbell NR, Bakhoum SF, Setty M, Lavallée V-P, Xie Y, Masilionis I, Carr AJ, Kottapalli S, et al. 2020. Regenerative lineages and immune-mediated pruning in lung cancer metastasis. *Nat Med* **26:** 259–269. doi:10.1038/s41591-019-0750-6

Liu T, Hu B, Choi YY, Chung M, Ullenbruch M, Yu H, Lowe JB, Phan SH. 2009. Notch1 signaling in FIZZ1 induction of myofibroblast differentiation. *Am J Pathol* **174:** 1745–1755. doi:10.2353/ajpath.2009.080618

Miranda KC, Huynh T, Tay Y, Ang Y-S, Tam W-L, Thomson AM, Lim B, Rigoutsos I. 2006. A pattern-based method for the identification of microRNA binding sites and their corresponding heteroduplexes. *Cell* **126:** 1203–1217. doi:10.1016/j.cell.2006.07.031

Nabhan AN, Brownfield DG, Harbury PB, Krasnow MA, Desai TJ. 2018. Single-cell Wnt signaling niches maintain stemness of alveolar type 2 cells. *Science* **359:** 1118–1123. doi:10.1126/science.aam6603

Obenauf AC, Massagué J. 2015. Surviving at a distance: organ-specific metastasis. *Trends Cancer* **1:** 76–91. doi:10.1016/j.trecan.2015.07.009

Orimo A, Gupta PB, Sgroi DC, Arenzana-Seisdedos F, Delaunay T, Naeem R, Carey VJ, Richardson AL, Weinberg RA. 2005. Stromal fibroblasts present in invasive human breast carcinomas promote tumor growth and angiogenesis through elevated SDF-1/CXCL12 secretion. *Cell* **121:** 335–348. doi:10.1016/j.cell.2005.02.034

Pankova D, Chen Y, Terajima M, Schliekelman MJ, Baird BN, Fahrenholtz M, Sun L, Gill BJ, Vadakkan TJ, Kim MP, et al. 2016. Cancer-associated fibroblasts induce a collagen crosslink switch in tumor stroma. *Mol Cancer Res* **14:** 287–295. doi:10.1158/1541-7786.MCR-15-0307

Park S-M, Gaur AB, Lengyel E, Peter ME. 2008. The miR-200 family determines the epithelial phenotype of cancer cells by targeting the E-cadherin repressors ZEB1 and ZEB2. *Genes Dev* **22:** 894–907. doi:10.1101/gad.1640608

Park CY, Jeker LT, Carver-Moore K, Oh A, Liu HJ, Cameron R, Richards H, Li Z, Adler D, Yoshinaga Y, et al. 2012. A resource for the conditional ablation of microRNAs in the mouse. *Cell Rep* **1:** 385–391. doi:10.1016/j.celrep.2012.02.008

Pelossof R, Fairchild L, Huang C-H, Widmer C, Sreedharan VT, Sinha N, Lai D-Y, Guan Y, Premsrirut PK, Tschaharganeh DF, et al. 2017. Prediction of potent shRNAs with a sequential classification algorithm. *Nat Biotechnol* **35:** 350–353. doi:10.1038/nbt.3807

Pietras K, Östman A. 2010. Hallmarks of cancer: interactions with the tumor stroma. *Exp Cell Res* **316:** 1324–1331. doi:10.1016/j.yexcr.2010.02.045

Procopio M-G, Laszlo C, Al Labban D, Kim DE, Bordignon P, Jo S-H, Goruppi S, Menietti E, Ostano P, Ala U, et al. 2015. Combined CSL and p53 downregulation promotes cancer-associated fibroblast activation. *Nat Cell Biol* **17:** 1193–1204. doi:10.1038/ncb3228

Prosser HM, Koike-Yusa H, Cooper JD, Law FC, Bradley A. 2011. A resource of vectors and ES cells for targeted deletion of microRNAs in mice. *Nat Biotechnol* **29:** 840–845. doi:10.1038/nbt.1929

Quail DF, Joyce JA. 2013. Microenvironmental regulation of tumor progression and metastasis. *Nat Med* **19:** 1423–1437. doi:10.1038/nm.3394

Straussman R, Morikawa T, Shee K, Barzily-Rokni M, Qian ZR, Du J, Davis A, Mongare MM, Gould J, Frederick DT, et al. 2012. Tumour micro-environment elicits innate resistance to RAF inhibitors through HGF secretion. *Nature* **487:** 500–504. doi:10.1038/nature11183

Strell C, Paulsson J, Jin S-B, Tobin NP, Mezheyeuski A, Roswall P, Mutgan C, Mitsios N, Johansson H, Wickberg SM, et al. 2019. Impact of epithelial–stromal interactions on peritumoral fibroblasts in ductal carcinoma in situ. *JNCI J Natl Cancer Inst* **111:** 983–995. doi:10.1093/jnci/djy234

Su Q, Zhang B, Zhang L, Dang T, Rowley D, Ittmann M, Xin L. 2017. Jagged1 upregulation in prostate epithelial cells promotes formation of reactive stroma in the Pten null mouse

model for prostate cancer. *Oncogene* **36:** 618–627. doi:10.1038/onc.2016.232

Sun Y, Fan X, Zhang Q, Shi X, Xu G, Zou C. 2017. Cancer-associated fibroblasts secrete FGF-1 to promote ovarian proliferation, migration, and invasion through the activation of FGF-1/FGFR4 signaling. *Tumor Biol* **39:** 1–10.

Tammela T, Sanchez-Rivera FJ, Cetinbas NM, Wu K, Joshi NS, Helenius K, Park Y, Azimi R, Kerper NR, Wesselhoeft RA, et al. 2017. A Wnt-producing niche drives proliferative potential and progression in lung adenocarcinoma. *Nature* **545:** 355–359. doi:10.1038/nature22334

Winslow MM, Dayton TL, Verhaak RGW, Kim-Kiselak C, Snyder EL, Feldser DM, Hubbard DD, DuPage MJ, Whittaker CA, Hoersch S, et al. 2011. Suppression of lung adenocarcinoma progression by Nkx2-1. *Nature* **473:** 101–104. doi:10.1038/nature09881

Yu J-R, Tai Y, Jin Y, Hammell MC, Wilkinson JE, Roe J-S, Vakoc CR, Van Aelst L. 2015. TGF-β/Smad signaling through DOCK4 facilitates lung adenocarcinoma metastasis. *Genes Dev* **29:** 250–261. doi:10.1101/gad.248963.114

Zheng Y, de la Cruz CC, Sayles LC, Alleyne-Chin C, Vaka D, Knaak TD, Bigos M, Xu Y, Hoang CD, Shrager JB, et al. 2013. A rare population of $CD24^{+}ITGB4^{+}Notch^{hi}$ cells drives tumor propagation in NSCLC and requires Notch3 for self-renewal. *Cancer Cell* **24:** 59–74. doi:10.1016/j.ccr.2013.05.021